Snowfall Limit Forecasts and Hydrological Modeling

CARA TOBIN, ANDREA RINALDO, AND BETTINA SCHAEFLI

Laboratory of Ecohydrology ECHP/IIE/ENAC, Ecole Polytechnique Fèdèrale de Lausanne, Lausanne, Switzerland

(Manuscript received 22 November 2011, in final form 27 April 2012)

ABSTRACT

Hydrological flood forecasting in mountainous areas requires accurate partitioning between rain and snowfall to properly estimate the extent of runoff contributing areas. Here a method to make use of snowfall limit information—a standard output of limited-area models (LAMs)—for catchment-scale hydrological modeling is proposed. LAMs consider the vertical, humid, atmospheric structure in their snowfall limit calculations. The proposed approach is thus more physically based than inferring snowfall limit estimates based on (dry) ground temperature measurements, which is the standard procedure in most hydrological models. The presented case study uses forecast reanalyses from the Consortium for Small-Scale Modeling (COSMO) limited-area model as input for discharge simulation in a topographically complex catchment in the Swiss Alps. Results suggest that the use of COSMO snowfall limits during spring snowmelt periods can provide more accurate runoff simulations than routine procedures, with practical implications for operational hydrology in Alpine regions.

1. Introduction

It has long been recognized that Alpine precipitation is controlled by numerous meteorological factors. Most notably, the observed precipitation type is influenced by latent heat (Unterstrasser and Zaengl 2006), thermal and moisture distributions, vertical atmospheric motion, and ice nuclei distributions (Bourgouin 2000). Relative humidity has been shown to highly impact the precipitation phase near the freezing point; Matsuo and Sasyo (1981) demonstrated snowfall with temperatures up to 4°C when the air was relatively unsaturated. In general, the energy necessary for phase transformation (i.e., melting and evaporation) extracts latent heat from the atmosphere with limits depending on the relative humidity. The wet-bulb temperature gives an indication of the air humidity as it measures the lowest temperature that can be achieved by the evaporation of water from a parcel of moistened air. It is classically measured with a psychrometer whose bulb is moistened such that air near the wet bulb is cooled by the transfer of heat from the air required to evaporate the water. Together with the dry-bulb temperature, the wet-bulb temperature determines saturation; the wet-bulb temperature is always lower than the dry-bulb temperature because of evaporative cooling until atmospheric saturation is achieved, where both temperatures are equal (Schneider et al. 2011).

The wet-bulb temperature of different atmospheric layers plays a significant role in the initiation, melting, and freezing of hydrometeors, thereby acting as an influential factor in the prediction of the altitude where the transition from snow to rainfall occurs [i.e., snowfall limit (SL)]. Accordingly, the wet-bulb temperature is used in different precipitation phase models for forecast purposes (Bourgouin 2000; Graham and Evans 2011). In contrast, computation of SLs within hydrological models is typically based on a spatial interpolation of dry ground temperatures with estimated lapse rates, neglecting both pressure and relative humidity (e.g., Hingray et al. 2010; Fundel and Zappa 2011), although a limited amount of hydrological studies use the wet-bulb temperature for SL calculations (Blöschl et al. 1991; Haiden et al. 2011). Because the phase of precipitation depends on the conditions in the location where it is formed as well as ground conditions, the typical dry temperature interpolation can provide considerably erroneous information, particularly if lapse rates are treated as constant in time (Tobin et al. 2011; Minder et al. 2010).

Current snow research for hydrological modeling purposes focuses on the prediction of snow water equivalent

Corresponding author address: Cara Tobin, EPFL and C. Greene Consulting, Lausanne, Switzerland.
E-mail: ctobin@stanfordalumni.org

DOI: 10.1175/JHM-D-11-0147.1

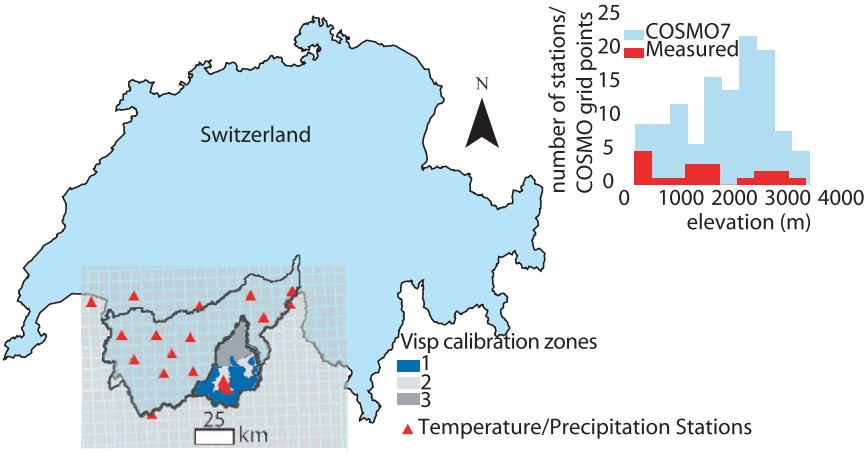

FIG. 1. Location of the Visp in Switzerland with the COSMO7 grid, the hourly temperature and precipitation stations utilized, and the zones used for GLUE calibration. Only COSMO grid points located within the large black polygon line (indicating the Valais region) were used. (inset) Number of COSMO7 grid points and meteorological stations (with hourly data) vs their respective true ground elevations.

(Jonas et al. 2009) and snow-covered areas. Both predictions face two major challenges: full energy/mass balance approaches require a significant amount of measurement inputs such as radiation fluxes and water vapor pressure (Rohrer and Braun 1994; Lehning et al. 2006) and typically there exist few point measurements available for generalized model calibration and validation. To address this last problem, numerous studies have focused on the use of remotely sensed snow-covered areas to improve snow simulation routines (Parajka and Blöschl 2008; Finger et al. 2011). In the context of real-time flood forecasting, however, updating model states with remotely sensed snow cover information at different spatiotemporal resolutions is relatively complex (Dozier 2011). Flood forecasting models are driven by limited-area models (LAMs) to provide predictions for meteorological variables. In this context, a straight-forward option to better define the snow component of hydrological models is to directly use SL output from LAMs as an input to hydrological modeling to improve the snow/rain delimitation.

LAM temperature and precipitation forecasts have previously been used to update hydrological models (Akhtar et al. 2008) and cross validation of LAMs with measured ground data has been used to compute snowfall accumulation forecasts (Haiden et al. 2011). It is well understood that LAM output variables contain error (Pappenberger et al. 2011). However, to the authors' knowledge, SL output, specifically, has not yet been tested in terms of its viability for hydrological modeling. This study therefore attempts to use LAM SLs as hourly input to a catchment-scale hydrological model. The main goal for this study is to improve flood forecasting for a suitably complex catchment in the Swiss Alps characterized by strong topographic gradients where an incorrect snow/rainfall limit on daily or subdaily time scales (Mezghani and Hingray 2009) typically implies a significant over- (or under)estimation of the source catchment areas contributing to runoff and infiltration, with a view to operational hydrology.

2. Materials and methods

a. Study site and meteorological data

The analyses described herein refer to an Alpine catchment located in the Swiss region of the Valais, the Visp catchment (800 km^2), drained by the Vispa River (Fig. 1). Highest annual discharges in the Vispa occur during spring and summer because of snow and ice melt. The Visp catchment has steep slopes and high peaks (Matterhorn, 4478 m); soil cover is predominantly sandy loam and approximately 33% of the surface area is covered by glaciers.

Dry-bulb temperature and precipitation measurements were obtained from the MeteoSwiss Automatische Wetterbeobachtungsnetz der Schweiz (ANETZ) meteorological network (Gutermann 1986). The use of other Snow and Avalanche Research Institute (SLF) temperature stations was initially considered. However, these stations are installed in predominantly exposed areas for wind and snow observations (Lehning et al. 2002). Accordingly, they are not considered representative of average local temperature conditions and have not been used in this study. Rather, all MeteoSwiss stations indicated

in Fig. 1 are used as inputs to the hydrological model. These stations are located in or near the Valais region (indicated by the dark outline). The Valais region, corresponding to the catchment of the Rhone River, which receives the Vispa discharge, is relevant for the spatial interpolation of meteorological variables because it corresponds to the scale of typical weather phenomena in this area.

b. COSMO models and output

The Consortium for Small-Scale Modeling (COSMO) models, COSMO2 and COSMO7, are nonhydrostatic limited-area models integrated at horizontal resolutions of 2×2 km^2 and 6.8×6.8 km^2, respectively (Addor et al. 2011). Both models use a generalized terrain-following height coordinate with user-defined grid stretching in the vertical. Data assimilation is performed using nudging to update model states based on observations from radio soundings and pilots, conventional surface station data (such as the ANETZ temperature and precipitation data used here), aircraft meteorological data relays (AMDARs) (i.e., airplane data), data from ships and buoys, wind profilers, and radar data (for COSMO2 only). The forecast ranges for COSMO2 and COSMO7 are 24 and 72 h, respectively.

Grid-scale clouds are resolved in the COSMO models by using a scheme including ice clouds as a prognostic variable, which leads to a function describing the fraction of cloudiness. The partitioning of water into water vapor, the nonprecipitating categories of cloud water and cloud ice, and the precipitating categories [i.e., rain, snow, and graupel (graupel, in the case of COSMO2 only)] is performed by a prognostic scheme where the full hydrological budget equations for precipitating hydrometeors are solved (including 3D advective transport). Further details on the parameterization of cloud and precipitation physics, boundary layer turbulence, and surface fluxes are detailed in COSMO (2011).

The differences between COSMO2 and COSMO7 relate to their driving forces, their configurations, their reinitialization frequencies, and their treatment of convection. The initial and lateral boundary conditions (i.e., the driving models) for COSMO7 and COSMO2 are the Integrated Forecasting System (IFS) from ECMWF and COSMO7, respectively. COSMO7 has 45 vertical layers while COSMO2 has 60 layers, both with model tops set at 20 hPa. Below 3 km in the atmospheric column where melting generally takes place, the COSMO model's vertical grid spacing becomes progressively finer closer to the ground. Vertical differences range from approximately 1200 m between the top layers at 3 km to a difference of approximately 20 m at the ground. The frequency of reinitialization of COSMO2 is every 3 h (i.e., eight runs per day) whereas the COSMO7 model is reinitialized twice per day. The COSMO7 model parameterizes both deep and shallow convection while COSMO2 considers only shallow convection because its high resolution enables the explicit resolution of deep convection, which reduces model uncertainty (Weusthoff et al. 2010). COSMO7 deep convection is parameterized by the mass flux scheme of Tiedtke (1989).

Numerous research endeavors have demonstrated the success of the COSMO products in the Mesoscale Alpine Programme Demonstration of Probabilistic Hydrological and Atmospheric Simulation of Flood Events in the Alpine Region (MAP D-PHASE) project. Bauer et al. (2011) showed that the COSMO models are capable of forecasting correct distributions of precipitation, particularly for low precipitation thresholds. In complex terrain, COSMO2 has been shown to yield better precipitation forecasting performance than coarser COSMO products because of its more frequent initialization and its explicit calculation of deep convection (Weusthoff et al. 2010; Ament et al. 2011). Similarly, flood peaks have been proven to be accurately captured with short-term COSMO2 forecasts (Zappa et al. 2011).

For this case study, 24-h periods from COSMO2 and COSMO7 models are analyzed. Because the COSMO7 product provides 72-h forecasts, the data are reconstructed by using the first 24 h of each reanalysis forecast after a 6-h initialization period. This process uses the most recent forecast information (i.e., the smallest lead time predicted) and reduces sensitivity to state variable initialization. Accordingly, COSMO7 model output is used from hour 6 through hour 30, omitting the forecast information predicting further into the future. COSMO7 data was available for 2008 and 2009, while COSMO2 was available for 2009.

The SLs used in these analyses are the output of COSMO. They are computed based on the wet-bulb temperature at every point of the horizontal grid using an empirical method developed at MeteoSwiss (Häberli et al. 2008; M. Stoll 2011, personal communication). In this approach, SLs are calculated by using a loop from top to bottom over all model layers below 8000 m searching for the first layer with a wet-bulb temperature $\geq$1.3°C. The elevation corresponding to the 1.3°C isotherm is assumed to be the threshold for snowfall; above this temperature the precipitation falls as rain and vice versa. Model output of the SL is provided as an elevation (in m MSL) for each COSMO (x, y) grid point. All COSMO grid points in the Valais are used to provide the SL input to the hydrological model (see Fig. 1).

The empirical wet-bulb temperature threshold of 1.3°C has been determined by MeteoSwiss based on their forecasters' experience (Häberli et al. 2008) and is also used

by the German Meteorological Service (DWD) (Schulz and Schattler 2009). Other authors suggest different values; for example, Steinacker (1983) has proposed the threshold value to be close to 1.0°C. It should be noted that the meteorological services use the empirical wet-bulb-based SL rather than directly characterizing the COSMO SL from the model's 3D rain and snow fields. The resulting predicted SL will be different from the actual SL since the estimation procedure neglects many (micro)physical processes and in particular any local variations of hydrometeor melting conditions (related to vertical winds, hydrometeor size, or fall speed). The simplified procedure is, however, preferred in operational forecasting environments because of its robustness and greater computational time efficiency (Häberli et al. 2008; Graham and Evans 2011).

c. Hydrological model

Hydrological simulations are based on the semidistributed, reservoir-based Glacier–Snowmelt Soil Contribution (GSM-SOCONT) model (Schaefli et al. 2005; Tobin et al. 2011) that has been implemented for operational flood forecasting (Jordan et al. 2008) in the upper Rhone River catchment by the Valais and Vaud cantons (see Jordan 2007 and Hingray et al. 2010 for model details and calibration parameters). Catchment limits are defined according to topography described by a 25-m-resolution digital terrain model (DTM). Hydraulic works (i.e., water diversions due to pumping and piping configurations) act as physical constraints in the model. Subcatchments are further subdivided into elevation bands to account for the significant ranges in altitude. Snow and ice melt discharges are computed with the degree-day method (Martinec and Rango 1986). Following Schaefli et al. (2005), corresponding discharges from glacier-covered catchment parts are modeled with a linear reservoir approach. Rainfall/meltwater–runoff transformation for glacier-free parts is completed with three reservoirs—one for fast overland flow and two for slower contributions. Overland flow is modeled via the Manning–Strickler equation—the standard flow resistance relation linking velocity, slope, and hydraulic features for open channel flows (Chanson 2004). Subsurface flow is modeled with two linear reservoirs connected through a constant recharge. The second subsurface reservoir has been added to the original GSM-SOCONT model to provide a rapid, yet delayed flow contribution in the subsurface layer [similar to the interflow in the well-known Hydrologiska Byråns Vattenbalansavdelning (HBV) model] (Bergstrom 1995).

Overland flow is defined by the Strickler coefficient ($m^{1/3}\ s^{-1}$), interflow is defined by the interflow residence time coefficient (hours), and baseflow is defined by the subsurface residence time coefficient (days). These residence time coefficients affect the form of the hydrograph. Snow and glacier melt are described by degree-day factors, which determine how much melt per °C per day contributes to the equivalent precipitation that infiltrates or is routed in the channels (Martinec and Rango 1986). The water equivalent determined by these factors affects the volume and peak of the hydrograph.

Hydrologic computations are performed at an hourly time scale to capture the dynamic flood responses in the Alps. The operational model uses inverse distance weighting (IDW) to interpolate measured precipitation to the centroid of each subcatchment. IDW is also used to interpolate the elevation-detrended temperature in the x, y space, which is subsequently interpolated to the centroid elevation z of each elevation band with a time-variable lapse rate (Tobin et al. 2011; Blandford et al. 2008; Minder et al. 2010). In using COSMO SL input, each elevation band is assigned the closest COSMO grid point using MeteoSwiss procedures where the Euclidian distance in the horizontal is summed with the vertical difference multiplied by a correction factor. The correction factor is used to make both the vertical and horizontal differences have relatively equal importance in spite of the vertical distance being typically an order of magnitude less (Kaufmann 2008).

d. Snowfall limit methods

In the hydrological model, the standard calculation of the amount of liquid versus solid precipitation per elevation band with centroid elevation z is determined based on a temperature threshold approach that computes the ratio of rainfall to total precipitation, α, based on two critical temperatures (T_{c1}, T_{c2}) and a linear transition within the range $\Delta T_c = T_{c2} - T_{c1}$—a standard method in hydrology (Schaefli et al. 2005; Kienzle 2008) and in agreement with observations (Rohrer and Braun 1994). This approach shall hereafter be referred to as the "Ground" method to indicate its use of dry-bulb ground temperatures alone for SL calculation:

$$\alpha(z) = \begin{cases} 0 & T(z) < T_{c1} \\ \dfrac{T(z) - T_{c1}}{\Delta T_c} & T_{c1} \le T(z) \le T_{c2} \\ 1 & T(z) > T_{c2} \end{cases}. \quad (1)$$

In accordance to observed snow/rain distributions (Rohrer and Braun 1994), the critical temperatures are set to $T_{c1} = 0$°C and $T_{c2} = 2$°C.

To overcome the limitations of the Ground method, a new method is proposed here, based on the snowfall limit height, H_{SL} (m MSL), predicted by COSMO, which

we call the COSMO method. The basic principle of a temperature range $\Delta T_c = 2°C$, for which snowfall and rainfall occur simultaneously, is maintained. However, in the COSMO method, the ratio α is estimated based on H_{SL} in three steps:

(i) The range of elevations over which snowfall and rainfall occur, ΔH, is computed as

$$\Delta H = H_0 - H_1 = \frac{\Delta T_c}{\ell}, \tag{2}$$

where $l > 0$ is the time-variable lapse rate estimated from the COSMO temperature field.

It is assumed, as before, that α varies linearly in this range; for elevations $z > H_0$ no rainfall occurs ($\alpha = 0$) and for $z > H_1$ only rainfall occurs ($\alpha = 1$).

(ii) Assuming furthermore that at the elevation H_{SL} 75% of the precipitation falls as snow [i.e., $\alpha(H_{SL}) = \alpha_{SL} = 0.25$], the elevations H_1, H_0 can be related to H_{SL} as follows:

$$\begin{aligned} H_1 &= H_{SL} - (1 - \alpha_{SL})\Delta H \\ H_0 &= H_{SL} + \alpha_{SL}\Delta H. \end{aligned} \tag{3}$$

(iii) These elevations are then used to determine $\alpha(z)$ for a given elevation band:

$$\alpha(z) = \begin{cases} 0 & z > H_0 \\ \dfrac{z - H_1}{H_0 - H_1} & H_0 \geq z \geq H_1 \\ 1 & z < H_1 \end{cases}. \tag{4}$$

The sensitivity of the range in temperatures ΔT_c was previously tested with the hydrological model. Results indicated that the range from 0° to 2°C provides the best performance in terms of defining the transition between rain and snow in this Alpine region. This range also corresponds to the findings of other studies within Switzerland (Rohrer and Braun 1994). It is assumed here that the range performs well for both methods.

Note that there is generally no clear definition of what the SL actually means (Steinacker 1983); it represents the transition from liquid to solid precipitation, which we assume here to take place at 25% rainfall. For the Ground method, this transition (25% rainfall) corresponds to the threshold of 0.5°C (dry bulb).

Both methods account for their own respective lapse rate in their calculations of the SL. A preliminary analysis of the lapse rates demonstrated that some values can be negative because of the presence of inversion layers in the valley of the Alpine region. It is known that inversion layers can occur during the winter up to elevations of 1000 m in the European Alps (Agrawala et al. 2007). Mean negative lapse rates were noted for some periods on the order of days in 2008 and 2009, respectively. To compare the SL methods under typical meteorological conditions and for the sake of simplicity in this analysis, negative lapse rates were ignored. A positive lapse rate from the previous time step was maintained in the SL calculations.

e. Hydrological model calibration and validation

Two different hydrological models are set up by combining the snow/rainfall–runoff module with each of the above SL limit computation methods. Only COSMO7 model output is used as input to the model in order to have 2 years of input for calibration and validation. These two models are calibrated independently with measured discharge at the Visp catchment outlet using the generalized likelihood uncertainty estimation (GLUE) approach (Beven and Freer 2001), which is a well-established Monte Carlo simulation method used to assess the plausibility of hydrological simulations (Pappenberger et al. 2007). This approach assumes that, given the modeler's imperfect knowledge of a system, there are many parameter sets that can be considered equally good simulators of the system. In the hydrologic literature, equally good parameter sets are termed equifinal (Beven 2006). As a result, instead of a single hydrological simulation corresponding to a single best parameter set, an ensemble of simulations corresponding to an ensemble of acceptable parameter sets is retained. These parameter sets are identified by generating a high number of random parameter sets drawn from a prior parameter range and by retaining those sets that have a model performance above or below a certain threshold criteria (see Table 1). For the calibration, the catchment is divided into three zones with similar physical characteristics (e.g., presence of glaciers) (see Fig. 1). The model performance criteria are the Nash–Sutcliffe efficiency (NSE; Nash and Sutcliffe 1970) and the mean absolute residual error (MARE). The theoretical optimums are 1 for the NSE and 0 for the MARE criterion and their respective thresholds for acceptability are ≥ 0.8 and ≤ 0.3. The best parameter sets under these two criteria were selected by taking the intersection of the parameter sets, which satisfied both thresholds of acceptability.

These performance criteria are computed over only medium to high flow events in order to exclude the daily fluctuations during low flow situations caused by hydropower operations. Simulations herein could not incorporate these fluctuations because the reservoir storage and release mechanisms are not public information. The two models (one for each SL method) are calibrated independently to match the mean flow over the entire

TABLE 1. Prior parameter range for Monte Carlo simulations with and without the best-performing parameter sets per zone for both the case of incorporating COSMO snowfall limits (COS) and using dry-bulb ground-temperature-derived snowfall limits (GND).

Parameter	Prior	Zone 1001		Zone 1002		Zone 1003	
		COS	GND	COS	GND	COS	GND
Degree-day glacier (mm day^{-1} °C^{-1})	1–8	1.7	2.0	6.8	6.1	3.7	6.4
Degree-day snow (mm day^{-1} °C^{-1})	3–9	4.0	6.4	8.0	8.4	5.9	5.4
Interflow residence time (h)	5–200	95	181	12	60	8	26
Subsurface residence time (days)	10–60	33	32	33	32	32	32
Recharge (mm day^{-1})	0.1–5	1.3	2.1	1.0	0.9	1.7	1.5
Strickler coefficient (m$^{1/3}$ s^{-1})	10–150	100	105	14	20	50	25

calibration period and the peak flows for the critical flow event at the end of May 2008. The May 2008 event was considered a high flow event, without, however, being an alert-level flood event (Garcia Hernández et al. 2009). The model is validated on the discharge time series for the June 2008 and April 2009 events by performing a continuous simulation through 2008 and 2009. The range of prior parameter values was determined based on accepted values from literature and use of the model in the Valais since 2005. To hot start the model (i.e., assign a spinup period that allows the choice of the initial parameter sets to be immaterial) and account for the beginning of the hydrological year, the initial conditions for October–December of 2007 were obtained by running the model with measured data only (since no COSMO data was available). One hundred acceptable parameter sets were selected based on the NSE and MARE criteria for the May 2008 event by retaining the parameter sets that adhered to both the MARE and NSE thresholds of acceptability ($\geq$0.8 for NSE and $\leq$0.3 for MARE).

f. Snow cover validation

For additional validation purposes, we use a daily Interactive Multisensor Snow and Ice Mapping System (IMS) snow coverage image provided by the National Oceanographic and Atmospheric Administration (NOAA) National Ice Center (30 May 2008) and two daily National Snow and Ice Data Center (NSIDC) Moderate Resolution Imaging Spectroradiometer (MODIS) MOD10-L2 satellite images (1 July 2008 and 1 May 2009) to validate the snow coverage for the three events.

IMS images (4 km $\times$ 4 km resolution) are produced based on a composite of satellite images using visible, passive, and microwave wavelengths (see National Ice Center 2008, Helfrich et al. 2007, and Pullen et al. 2011 for details). A prime advantage of the microwave sensors is their ability to penetrate clouds. The IMS determination of ''snow/no-snow coverage'' is indicated when at least 40% of a grid cell is covered by snow of any depth.

MOD10-L2 images (500 m $\times$ 500 m resolution) are *Terra* satellite images of snow cover (see Hall et al. 2006 for details). The snow mapping algorithm classifies pixels as snow, snow-covered lake ice, cloud, water, land, or other based on the reflectance or radiance properties in each 500-m pixel using the normalized difference snow index (NDSI) ratio—that is, the difference in reflectance of snow in the visible and near-infrared wavelengths (Hall et al. 2006). Fractional snow cover maps are based on the regression technique of Salomonson and Appel (2004). The MODIS products calculate the fractional area (in percent) of each pixel covered by snow for both land and inland water bodies not covered by clouds.

A comparison of MODIS and IMS snow coverage estimates on a daily basis with snow measurement stations [e.g., snow telemetry (SNOTEL)] indicated that the accuracy of IMS snow coverage increases with increasing snow cover and MODIS images tend to overestimate snow cover in the accumulation season (Brubaker et al. 2005). Most relevant to this analysis, Brubaker et al. (2005) demonstrated that IMS detected snow-free cells at a rate between 95% and 100% in the spring season relative to measurement data. Similarly, snow-free cells as indicated by MODIS were confirmed 100% by station data throughout the year 2000.

Both types of snow images provide a means to distinguish between snow-covered and snow-free areas. In this study, they are used to validate the simulated snow cover at the time of the calibration and validation events. Since the model yields snow heights (in terms of water equivalent) per elevation band rather than absence or presence of snow per pixel, this validation requires a post-treatment of the simulation results in two steps: (i) the simulated mean snow-covered area of the catchment is computed and (ii) the corresponding snow-covered pixels are estimated based on the hypsometric curve of the catchment. As both the model and snow cover images integrate snow cover over the winter season, it is assumed here that this validation approach is suitable.

It should be noted that this study attempted to validate all rain events with these MODIS images because they have the same resolution as the hydrological model input interpolations (i.e., 500 m). However, MODIS

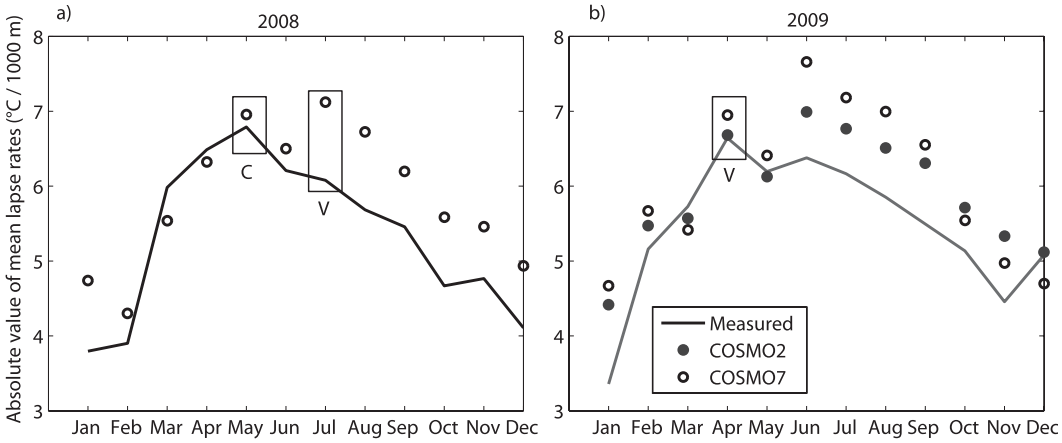

FIG. 2. Comparison of the monthly mean of the absolute value of the variable lapse rates obtained from COSMO2 (2009 only) and COSMO7 temperatures and from measured hourly ground temperature data for (a) 2008 and (b) 2009. The rectangles over May 2008, July 2008, and April 2009 indicate the calibration ("C") and validation ("V") periods.

images can only be used on clear days immediately following rain events because of the inability of infrared to penetrate clouds. For the May 2008 event, a coarse 4-km-resolution IMS satellite image was the only validation image available because small rain events followed the event and hindered visibility.

3. Results

a. COSMO and ground station data comparison

A comparison of ground station versus COSMO reanalysis temperatures demonstrates that both datasets show strongly time-varying lapse rates (Fig. 2). The lapse rates might be biased for both data sources: For observed temperatures, this is primarily due to the concentration of hourly gauges within the elevation range of 500–1000 m MSL (Frei and Schär 1998) (Fig. 1). For COSMO outputs, this can be related to the coarseness of the resolution, which prevents an accurate parameterization of a detailed heat balance (Leimer et al. 2011), and to the fact that a grid point cannot be identified with a real-world location because of the different model orography. Both of these factors also partly explain the difference between COSMO2 and COSMO7 predictions. In spite of the different sources of bias, these lapse rates can be considered reasonable; they show the same, expected, variation with consistently lower lapse rates in winter and steeper rates in spring and early summer (Rolland 2003; Blandford et al. 2008; Minder et al. 2010).

By looking more in detail at the particular months of May 2008, July 2008, and April 2009 (Fig. 2) (the two spring events and one summer flood event), differences emerge in the lapse rates estimated by the two data sources (COSMO and observed station data) through analysis of the mean lapse rates per month. In the months when the flood events occurred, the predicted mean hourly lapse rates are higher for the COSMO model output. With steeper lapse rates predicted by the COSMO stations, the SL can be predicted to be lower because lower temperatures are extrapolated to higher altitudes.

Similarly, a comparison of COSMO SLs with the 25% snowfall elevation obtained via the Ground method shows that there is a difference in the SLs calculated for all event months (Fig. 3). For the calibration and validation events, the mean of the monthly snow limits predicted by COSMO are lower. The wet-bulb threshold of 1.3°C for 25% of rainfall was apparently lower than the corresponding threshold of the Ground method, which is 0.5°C (dry bulb). For comparison purposes, we also computed the SL with COSMO dry-bulb temperatures and a snow/rain transition range of 0°–2°C. Figure 3 shows that the SLs computed with COSMO dry temperatures do not correspond to the SLs determined by the COSMO method (using wet-bulb temperatures). The differences between the SLs determined by the Ground method and the COSMO method are therefore due to a combined effect of contrasting lapse rates and the incorporation of relative humidity information. Furthermore, the time-varying differences between the wet-bulb- and dry-bulb-derived SLs for COSMO2 and COSMO7 suggest that the wet-bulb temperature cannot easily be replaced by a dry-bulb temperature SL estimation routine; if the bias were constant in time, one might propose to simply modify the snow/rain transition threshold for the dry temperature estimation.

b. Hydrological modeling

Before analyzing the simulation results of both SL methods, the plausibility of the calibrated parameter

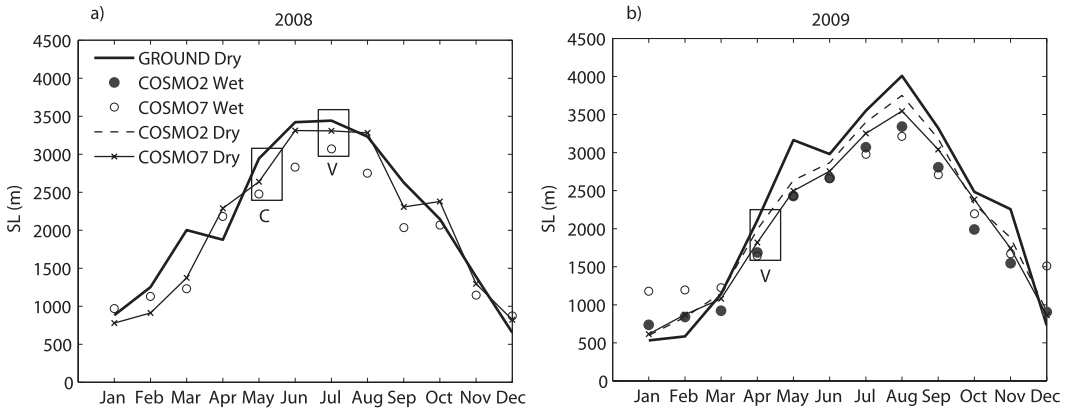

FIG. 3. Comparison of the mean monthly snowfall limits calculated with the COSMO2 (for 2009 only) and COSMO7 model outputs by the COSMO (wet) method and with observed ground temperatures by the ground (dry) method for (a) 2008 and (b) 2009. The mean monthly snow limits calculated according to the dry COSMO2 or COSMO7 temperatures are also indicated. The rectangles over May 2008, July 2008, and April 2009 snow limits indicate the C or V periods.

values should be analyzed. In fact, calibrating the rainfall–runoff transformation model combined with two different SL methods will necessarily lead to different parameter sets. However, it is expected that only the parameters directly related to fast runoff processes are very sensitive to the choice of the SL method and to the related timing and spatial distribution of water input during peak flow events. Slow runoff parameters should not vary significantly between the two model setups. This is confirmed by the two best parameter sets found for each of the methods (Table 1). As expected, the residence times of the slow subsurface stores and the recharge flux show similar values for the two methods. In contrast, the fast runoff parameters (the Strickler coefficient and the interflow residence time) vary strongly between the two methods, except the former for the highest elevation zone (zone 1; see Table 1), which has the highest glacier coverage (97%) and the smallest contribution to fast runoff processes. For this zone, the calibrated degree-day factor for snow also strongly varies between the methods. This might indicate an effect of compensation for imperfect liquid water input to the rainfall–runoff transformation module. A similar effect might be suspected for the strongly varying glacier degree-day factor for zone 3 that has an extremely small glacier coverage (1%).

The 100 best discharge simulations identified with the calibration procedure outlined in section 2e for each of two methods are compared to the observed discharge in Fig. 4. Note that the subdaily fluctuations around the base flow have been filtered from the observed discharge time series using the daily mean discharge. These fluctuations are in fact the result of unknown hydraulic regulations, which typically only take place during low and medium flow.

As shown in Fig. 4, the Ground method causes the nonflood event of May 2008 to be closer to the flood alarm level (Garcia Hernández et al. 2009) with some acceptable simulations crossing this threshold and the

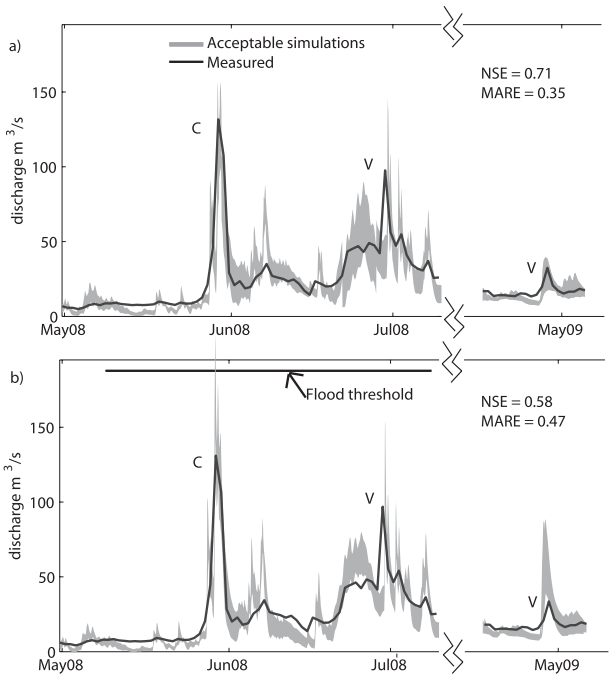

FIG. 4. (a) Discharge comparison for the calibration rain event in May 2008 and the validation events in July of 2008 and April of 2009 with the COSMO7 snowfall limit reanalysis forecasts (COSMO method). (b) Discharge comparison for the calibration rain event in May 2008 and the validation events in July of 2008 and April of 2009 with ground-temperature-based snowfall limit estimation (Ground method). Mean NSE and MARE values over the three events are shown. The measured discharge has been filtered to smooth daily fluctuations outside of the peak events. The C and V labels indicate either calibration or validation event.

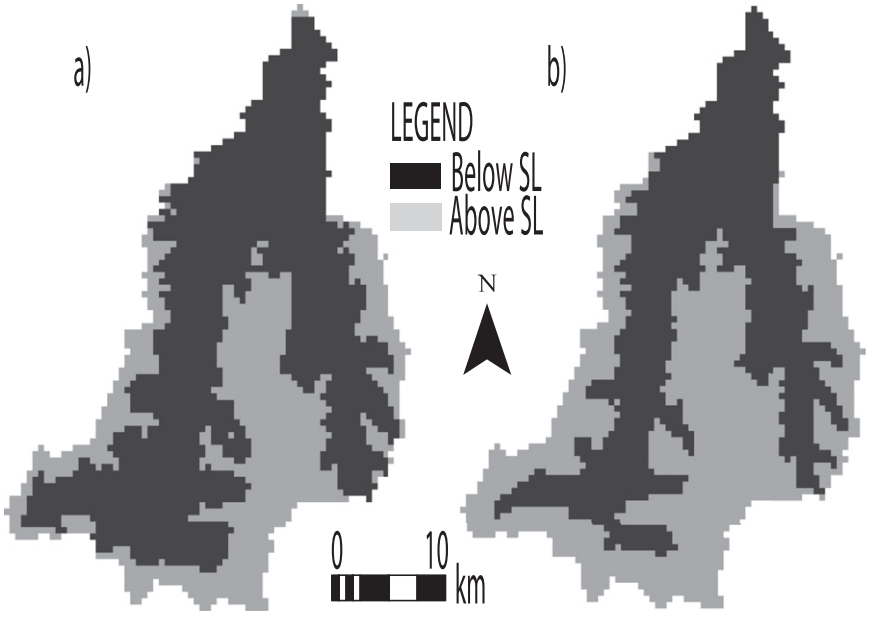

FIG. 5. SL for 30 May 2008 (i.e., the day with highest rainfall during the calibration event) as derived by (a) the ground and (b) the COSMO method.

mean of the acceptable simulations significantly exceeding the peak discharge.

With the COSMO method, this nonflood peak is more accurately predicted (see the NSE and MARE values in Fig. 4). Furthermore, the validation events also suggest that the COSMO method provides a more accurate snow/rainfall partitioning as evidenced by a better reproduction of the peaks, particularly for the April 2009 validation event. Note that the peak in July 2008 is approximately the same for both methods in spite of the different lapse rates and predicted snow limits. This result indicates that the SL plays a minor role during this summer period.

In fact, reliable SLs are most critical in spring when the soil storage and the snow layer of significant parts of

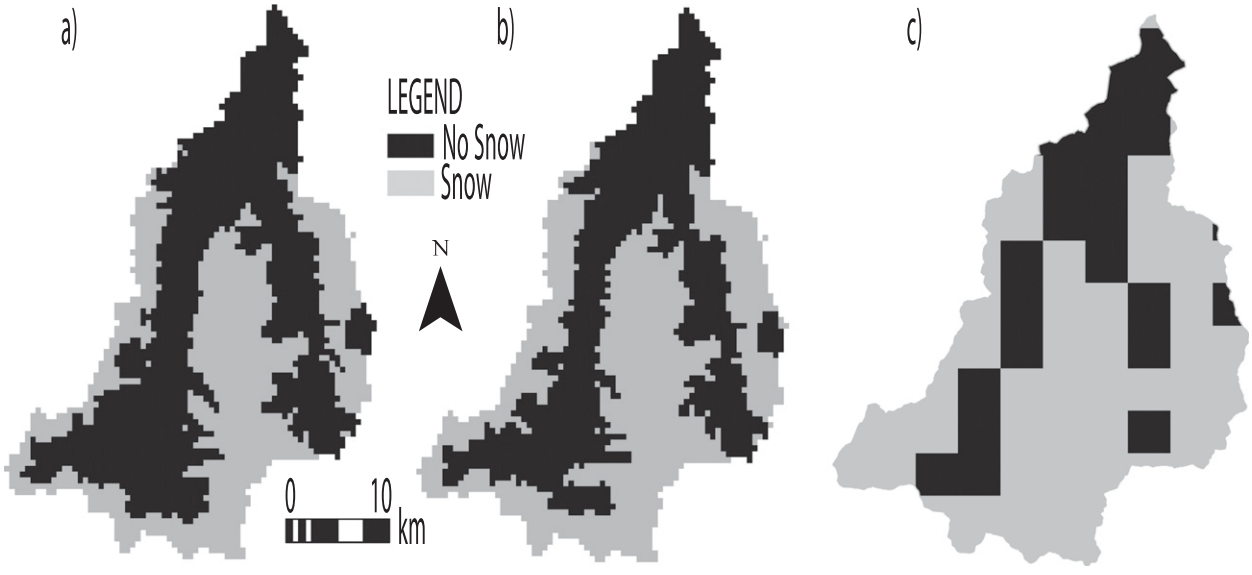

FIG. 6. Snow coverage (30 May 2008, calibration event) simulated with (a) hourly ground temperature stations (Ground method) and (b) COSMO7 snowfall limit forecasts (COSMO method). (c) Observed snow coverage (30 May 2008) based on an IMS snow coverage satellite image. The resolutions for (a),(b) are 500 m and for (c) is 4 km. Snow coverage percentages are (a) 44%, (b) 57%, and (c) 66%.

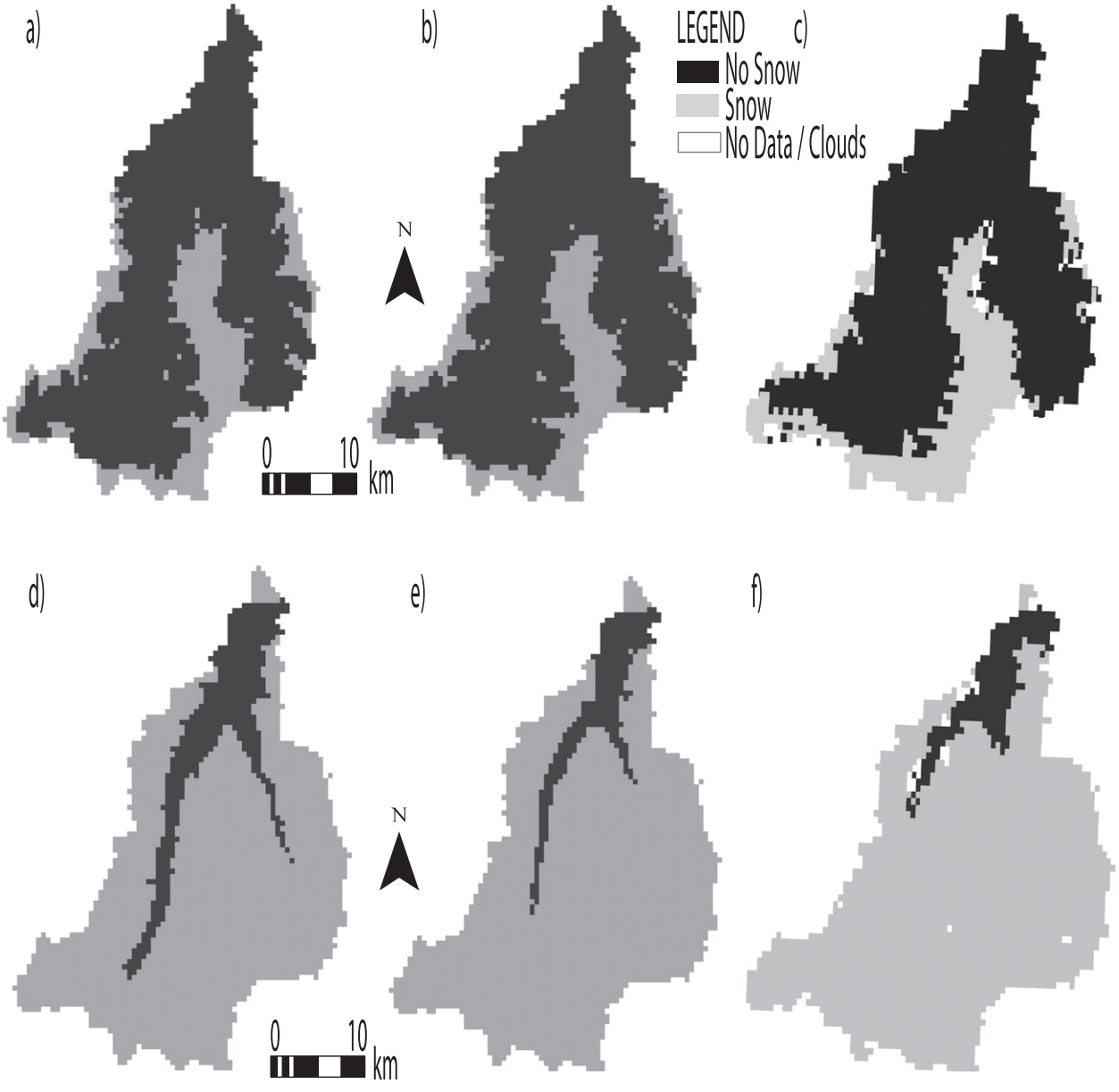

FIG. 7. Snow coverage for validation events, (a)–(c) July 2008 and (d)–(f) April 2009, simulated with (a),(d) hourly ground temperature stations (Ground method) and (b),(e) COSMO7 snowfall limit forecasts (COSMO method). Observed daily snow coverage from MODIS (MOD10-L2) satellites is shown for (c) 1 Jul 2008 and (f) 1 May 2009 (1 day after late April event). The resolution for all images is 500 m. Snow coverage percentages are (a) 25%, (b) 23%, (c) 24%, (d) 83%, (e) 89%, and (f) 91%.

the catchment are close to their saturation thresholds. At this time, the SL highly influences the runoff contributing area. Simultaneously, dry air temperature interpolation leads to SLs at higher elevations, which potentially produces a considerable overestimation of rainfall-experiencing catchment areas and an underestimation of snow receiving areas. This is illustrated in Fig. 5 showing a comparison of the SLs and the corresponding regions of the catchment receiving snow or rain for the day when the catchment received the most rainfall during the 2008 calibration event (30 May 2008). The SL is significantly lower with the COSMO method; the percentage of the catchment receiving snow is 51% and 36% for the COSMO and Ground methods, respectively.

A comparison of snow coverage for the last day of the 2008 calibration event in Fig. 6 shows a similar difference. With the COSMO method, the simulated snow-covered area corresponds to 57% of the catchment area

(Fig. 6b). In contrast, the Ground method generates 44% snow coverage (Fig. 6a). The use of a 4-km-resolution IMS satellite image (again, no finer, cloud-free-resolution images were available) to validate the simulated snow-covered area suggests a snow coverage for 66% of the catchment area (Fig. 6c).

Similar results can be seen with a comparison of snow coverage for the two validation events with MODIS (MOD10-L2) snow cover images at 500-m resolution. For both validation events the meteorological forcing interpolation resolution for the hydrological model and the satellite image resolution are the same.

In the case of the 2008 validation event, the snow coverage is very similar for the ground and COSMO methods (25% and 23% snow, respectively) (Figs. 7a,b) and close to that of the MODIS satellite image, which shows 24% snow coverage. This result is not unexpected in that the hydrographs are very similar for both methods.

In contrast, for the 2009 spring validation event, the snow coverage of the hydrological model output has a different spatial snow coverage than the satellite image along the valley branches (Fig. 7). Quantitatively, with the COSMO method, the simulated snow-covered area is 89% of the catchment area and corresponds well to the image snow-covered area at 91%. In contrast, the Ground method generates 83% snow coverage (Fig. 7d).

These results suggest that the Ground method underestimates the snow coverage for all three analyzed peak flow events. This could possibly explain why the surface residence parameter of the corresponding calibrated model is much higher than for the COSMO method [to obtain a similar hydrological response as the COSMO method, the Ground method model tries to retain the water longer in the considerably larger contributing (snow free) catchment part].

In conclusion, the calibration and validation images indicate that the proposed SL calculation method based on COSMO output has the potential to provide a more accurate data source for locating the snow/rain transition during spring and that solely ground temperature measurements may be inadequate to provide SL information during this time of the year. Future hydrological analyses will be conducted with more reanalysis data to validate and define the limits of the new method.

4. Conclusions

Hydrological flood forecasting models commonly compute the snow/rain transition elevation [snowfall limit (SL)] based on lapse rates derived from dry, ground temperature measurements. However, this study shows that such an approach can lead to significant inaccuracies in runoff computations due to the resulting erroneous spatial interpolations of the SLs. This is particularly critical in spring when (dry) air temperature-based SL estimation is highly likely to overestimate the SL elevation when a large part of the catchment is close to saturation. To overcome this problem, this paper has proposed a new method to estimate snow/rain transition limits for hydrological models based on SL output from COSMO limited-area models that are calculated with humidity and wet-bulb temperature information. Using a case study from the Swiss Alps, the new method is shown here to yield better estimates of contributing areas during spring peak flow events involving snowmelt. This, in turn, significantly improved runoff simulation. In conclusion, this work suggests that there exists a broad potential use for reanalysis datasets from limited-area models for hydrological modeling in Alpine regions.

Acknowledgments. This research was funded through the MINERVE 2008–11 project (Swiss Federal Office of the Environment, Cantons of Valais and Vaud). The authors also thank MeteoSwiss for the observed and COSMO data information and the National Environmental Satellite, Data, and Information Service (NESDIS) and the National Snow and Ice Data Center for the satellite images. Thanks also go to Dr. Andre Walser at MeteoSwiss for his clarifications on COSMO's calculations of the snowfall limit. Additional funding for the second and third authors was provided by the Swiss National Science Foundation SNF, Grant PZ00P2-126607, and the ERC Advanced Grant RINEC 22761.

REFERENCES

Addor, N., S. Juan, F. Fundel, and M. Zappa, 2011: An operational hydrological ensemble prediction system for the city of Zurich (Switzerland): Skill, case studies and scenarios. *Hydrol. Earth Syst. Sci.,* **15,** 2327–2347, doi:10.5194/hess-15-2327-2011.

Agrawala, S., B. Abegg, S. Jette-Nantel, F. Crick, and A. de Montfalcon, 2007: Climate change in the European Alps: Adapting winter tourism and natural hazards management. OECD Rep., 128 pp.

Akhtar, M., N. Ahmad, and M. Booij, 2008: Use of regional climate model simulations as input for hydrological models for the Hindukush–Karakorum–Himalaya region. *Hydrol. Earth Syst. Sci.,* **13,** 1075–1089.

Ament, F., T. Weusthoff, and M. Arpagaus, 2011: Evaluation of MAP D-PHASE heavy precipitation alerts in Switzerland during summer 2007. *Atmos. Res.,* **100,** 178–189.

Bauer, H., T. Weusthoff, M. Dorninger, V. Wulfmeyer, T. Schwitalla, T. Gorgas, M. Arpagaus, and K. Warrach-Sagi, 2011: Predictive skill of a subset of models participating in D-PHASE in the COPS region. *Quart. J. Roy. Meteor. Soc.,* **137,** 287–305, doi:10.1002/qj.715.

Bergstrom, S., 1995: The HBV model. *Computer Models of Watershed Hydrology,* V. P. Singh, Ed., Water Resource Publications, 443–476.

Beven, K., 2006: A manifesto for the equifinality thesis. *J. Hydrol.,* **320,** 18–36, doi:10.1016/j.hydrol.2005.07.007.

——, and J. Freer, 2001: Equifinality, data assimilation, and uncertainty estimation in mechanistic modelling of complex environmental systems using the glue methodology. *J. Hydrol.,* **249** (1–4), 11–29.

Blandford, T. R., K. S. Humes, B. J. Harshburger, B. C. Moore, V. P. Walden, and H. Ye, 2008: Seasonal and synoptic variations in near-surface air temperature lapse rates in a mountainous basin. *J. Appl. Meteor. Climatol.,* **47,** 249–261.

Blöschl, G., R. Kirnbauer, and D. Gutknecht, 1991: Distributed snowmelt simulations in an alpine catchment: 1. Model evaluation on the basis of snow cover patterns. *Water Resour. Res.,* **27,** 3171–3179, doi:10.1029/91WR02250.

Bourgouin, P., 2000: A method to determine precipitation types. *Wea. Forecasting,* **15,** 583–592.

Brubaker, K. L., R. T. Pinker, and E. Deviatova, 2005: Evaluation and comparison of MODIS and IMS snow-cover estimates for the continental United States using station data. *J. Hydrometeor.,* **6,** 1002–1017.

Chanson, H., 2004: *The Hydraulics of Open Channel Flow*. 2nd ed. Butterworth-Heinemann, 650 pp.

COSMO, 2011: Consortium for small-scale modeling. COSMO Tech. Rep., XX pp. [Available online at http://www.cosmo-model.org/content/model/documentation/core/default.htm.]

Dozier, J., 2011: Mountain hydrology, snow color, and the fourth paradigm. *Eos, Trans. Amer. Geophys. Union,* **92,** 373–374.

Finger, D., F. Pellicciotti, M. Konz, S. Rimkus, and P. Burlando, 2011: The value of glacier mass balance, satellite snow cover images, and hourly discharge for improving the performance of a physically based distributed hydrological model. *Water Resour. Res.,* **47,** W07519, doi:10.1029/2010wr009824.

Frei, C., and C. Schär, 1998: A precipitation climatology of the Alps from high-resolution rain-gauge observations. *Int. J. Climatol.,* **18,** 873–900.

Fundel, F., and M. Zappa, 2011: Hydrological ensemble forecasting in mesoscale catchments: Sensitivity to initial conditions and value of reforecasts. *Water Resour. Res.,* **47,** W09520, doi:10.1029/2010wr009996.

Garcia Hernández, J., P. Horton, C. Tobin, and J.-L. Boillat, 2009: MINERVE 2010: Prévision hydrométéorologique et gestion de crues sur le Rhône alpin. *Wasser Energ. Luft,* **4,** 297–302.

Graham, R., and M. Evans, 2011: Strength and weaknesses of P-type algorithms. NOAA warning decision training, NOAA Winter Weather, 30 pp. [Available online at http://www.wdtb.noaa.gov/courses/winterawoc/IC6/lesson2/part1/player.html.]

Gutermann, T., 1986: Das Automatische Wetterbeobachtungsnetz der Schweiz (ANETZ). Bericht Ed. MeteoSwiss, SMA, 17 pp.

Häberli, C., and Coauthors, 2008: Functions for the calculation of meteorological and climatological quantities used at the Swiss Meteorological Institute. Version 4.3, MeteoSwiss, Internal Report.

Haiden, T., A. Kann, C. Wittmann, G. Pistotnik, B. Bica, and C. Gruber, 2011: The Integrated Nowcasting through Comprehensive Analysis (INCA) system and its validation over the eastern Alpine region. *Wea. Forecasting,* **26,** 166–183.

Hall, D., G. Riggs, and V. Salomonson, 2006: MODIS/Terra snow cover 5-min L2 swath 500 m V005. National Snow and Ice Data Center, Boulder, CO, digital media. [Available online at http://nsidc.org/data/mod10_l2v5.html.]

Helfrich, S. R., D. McNamara, B. H. Ramsay, T. Baldwin, and T. Kasheta, 2007: Enhancements to, and forthcoming developments in the Interactive Multisensor Snow and Ice Mapping System (IMS). *Hydrol. Processes,* **21,** 1576–1586, doi:10.1002/hyp.6720.

Hingray, B., B. Schaefli, A. Mezghani, and Y. Hamdi, 2010: Signature-based model calibration for hydrological prediction in mesoscale Alpine catchments. *Hydrol. Sci. J.,* **55,** 1002–1016, doi:10.1080/02626667.2010.505572.

Jonas, T., C. Marty, and J. Magnusson, 2009: Estimating the snow water equivalent from snow depth measurements in the Swiss Alps. *J. Hydrol.,* **378** (1–2), 161–167, doi:10.1016/j.jhydrol.2009.09.021.

Jordan, F., 2007: Modéle de prévision et de gestion des crues: Optimisation des opérations des aménagements hydroélectriques á accumulation pour la réduction des débits de crue. Ph.D. dissertation, École Polytechnique Fédérale de Lausanne, 284 pp.

——, J. G. Hernández, J.-L. Boillat, and A. Schleiss, 2008: Flood forecast and flood management model: Optimization of the operation of storage power plants for flood routing. *11th Int. Interpraevent 2008 Conf. Proc.,* Vol. 1, Dornbirn, Austria, Interpraevent, 141–151.

Kaufmann, P., 2008: Association of surface stations to NWP model grid points. *COSMO Newsletter,* No. 9, DWD, Offenbach, Germany, 54–55.

Kienzle, S. W., 2008: A new temperature based method to separate rain and snow. *Hydrol. Processes,* **22,** 5067–5085, doi:10.1002/hyp.7131.

Lehning, M., P. Bartelta, B. Browna, and C. Fierza, 2002: A physical SNOWPACK model for the Swiss avalanche warning: Part III: Meteorological forcing, thin layer formation and evaluation. *Cold Reg. Sci. Technol.,* **35,** 169–184, doi:10.1016/S0165-232X(02)00072-1.

——, I. Völksch, D. Gustafsson, T. A. Nguyen, M. Stähli, and M. Zappa, 2006: ALPINE3D: A detailed model of mountain surface processes and its application to snow hydrology. *Hydrol. Processes,* **20,** 2111–2128, doi:10.1002/hyp.6204.

Leimer, S., P. Thorsten, S. Pfahl, and W. Wilcke, 2011: Towards a new generation of high-resolution meteorological input data for small-scale hydrological modeling. *J. Hydrol.,* **402,** 317–332.

Martinec, J., and A. Rango, 1986: Parameter values for snowmelt runoff modelling. *J. Hydrol.,* **84,** 197–219.

Matsuo, T., and Y. Sasyo, 1981: Non-melting phenomena of snowflakes observed in subsaturated air below freezing level. *J. Meteor. Soc. Japan,* **59,** 26–32.

Mezghani, A., and B. Hingray, 2009: A combined downscaling-disaggregation weather generator for stochastic generation of multisite hourly weather variables over complex terrain: Development and multi-scale validation for the Upper Rhone River basin. *J. Hydrol.,* **377** (3–4), 245–260, doi:10.1016/j.jhydrol.2009.08.033.

Minder, J., P. Mote, and J. Lundquist, 2010: Surface temperature lapse rates over complex terrain: Lessons from the Cascade Mountains. *J. Geophys. Res.,* **115,** D14122, doi:10.1029/2009JD013493.

Nash, J., and J. Sutcliffe, 1970: River flow forecasting through conceptual models part I—A discussion of principles. *J. Hydrol.,* **10,** 282–290, doi:10.1016/0022-1694(70)90255-6.

National Ice Center, 2008: IMS daily northern hemisphere snow and ice analysis at 4 km and 24 km resolution. National Snow and Ice Data Center, Boulder, CO, digital media. [Available online at http://nsidc.org/data/docs/noaa/g02156_ims_snow_ice_analysis/.]

Pappenberger, F., K. Beven, K. Frodsham, R. Romanowicz, and P. Matgen, 2007: Grasping the unavoidable subjectivity in calibration of flood inundation models: A vulnerability weighted approach. *J. Hydrol.,* **333** (2–4), 275–287, doi:10.1016/j.jhydrol.2006.08.017.

——, H. L. Cloke, A. Persson, and D. Demeritt, 2011: On forecast (in)consistency in a hydro-meteorological chain: Curse or blessing? *Hydrol. Earth Syst. Sci.,* **15,** 2391–2400, doi:10.5194/hess-15-2391-2011.

Parajka, J., and G. Blöschl, 2008: The value of MODIS snow cover data in validating and calibrating conceptual hydrologic models. *J. Hydrol.,* **358** (3–4), 240–258, doi:10.1016/j.jhydrol.2008.06.006.

Pullen, S., C. Jones, and G. Rooney, 2011: Using satellite-derived snow cover data to implement a snow analysis in the Met Office Global NWP Model. *J. Appl. Meteor. Climatol.,* **50,** 958–973.

Rohrer, M., and L. Braun, 1994: Long-term records of snow cover water equivalent in the Swiss Alps 2. Simulation. *Nord. Hydrol.,* **25,** 65–78.

Rolland, C., 2003: Spatial and seasonal variations of air temperature lapse rates in Alpine regions. *J. Climate,* **16,** 1032–1046.

Salomonson, V. V., and I. Appel, 2004: Estimating fractional snow cover from MODIS using the normalized difference snow index. *Remote Sens. Environ.,* **89,** 351–360.

Schaefli, B., B. Hingray, M. Niggli, and A. Musy, 2005: A conceptual glacio-hydrological model for high mountainous catchments. *Hydrol. Earth Syst. Sci.,* **2,** 73–117.

Schneider, S., M. Mastrandrea, and T. Root, Eds., 2011: *Encyclopedia of Climate and Weather.* 2nd ed. Oxford University Press, 1488 pp.

Schulz, J., and U. Schattler, 2009: Kurze beschreibung des lokalmodells Europa COSMO-EU (LME) und seiner datenbanken auf dem datenserver des DWD. German Meteorological Service (DWD), 67 pp.

Steinacker, R., 1983: Diagnose und prognose der schneefallgrenze. *Wetter Leben,* **35,** 81–90.

Tiedtke, A., 1989: A comprehensive mass flux scheme for cumulus parameterization in large-scale models. *Mon. Wea. Rev.,* **117,** 1779–1799.

Tobin, C., L. Nicotina, M. B. Parlange, A. Berne, and A. Rinaldo, 2011: Improved interpolation of meteorological forcings for hydrologic applications in a Swiss Alpine region. *J. Hydrol.,* **401,** 77–89, doi:10.1016/j.jhydrol.2011.02.010.

Unterstrasser, S., and G. Zängl, 2006: Cooling by melting precipitation in Alpine valleys: An idealized numerical modelling study. *Quart. J. Roy. Meteor. Soc.,* **132,** 1489–1508, doi:10.1256/qj.05.158.

Weusthoff, T., F. Ament, M. Arpagaus, and M. W. Rotach, 2010: Assessing the benefits of convection-permitting models by neighborhood verification: Examples from MAP D-PHASE. *Mon. Wea. Rev.,* **138,** 3418–3433.

Zappa, M., and Coauthors, 2011: MAP D-PHASE: Real-time demonstration of hydrological ensemble prediction systems. *Atmos. Sci. Lett.,* **9,** 80–87, doi:10.1002/asl.183.